

MRI Tagging of In Vivo Ventricular Function Reflects Changes in Myocyte Contractility and Calcium Handling in α -Dystrobrevin Knockout Mice

W. Li^{1,2}, W. Liu³, X. Yang¹, S. Banerjee¹, and X. Yu^{1,2}

¹Biomedical Engineering, Case Western Reserve University, Cleveland, OH, United States, ²Case Center for Imaging Research, Case Western Reserve University, Cleveland, OH, United States, ³Philips Research North America, Briarcliff Manor, NY, United States

Introduction

The dystrophin-glycoprotein complex (DGC), a membrane-associated structural protein complex that links the intracellular cytoskeleton to the extracellular matrix, plays an important role in the mechanical coupling and force transmission of myocyte contraction in heart. The disruption in DGC due to dystrophin deficiency leads to a severe muscle wasting disease, namely Duchene muscular dystrophy (DMD), as well as cardiomyopathy. However, our previous MRI tagging studies observed an unexpected increase in left ventricular contraction in the young mdx mice (a mouse model of DMD). The underlying mechanism for this increase is not understood. In addition to maintaining structural integrity, DGC also plays a signaling role by binding the sarcolemmal signaling protein, nNOS, through syntrophin and α -dystrobrevin. It has been shown that nNOS is displaced from DGC in mdx mouse (1), resulting in the disruption of both structural integrity and signaling function. Therefore, it is possible that the observed increase in ventricular contraction in young mdx mouse is due to changes in nNOS mediated signaling.

To test this hypothesis, we characterized α -dystrobrevin knockout ($adb^{n-/-}$) mice to explore the impact of altered DGC-associated signaling in the current study. Like mdx mouse, the DGC-associated nNOS is absent in $adb^{n-/-}$ mouse. However, the structural integrity is maintained. Therefore, $adb^{n-/-}$ mouse only presents disruption in DGC signaling role (1).

Methods

MR imaging: Two months old $adb^{n-/-}$ mice (n=5) and age matched control mice (n=7) were scanned on a Varian 4.7T scanner with a 2.5 cm surface coil. Tagged images of up to six short-axis slices were acquired from apex to base with 1 mm slice thickness. The tagging sequence used a SPAMM1331 sequence applied twice immediately after the ECG trigger, yielding a two-dimensional tag grid in imaging plane. The tagging sequence was followed by gradient-echo cine sequence with the following imaging parameters: TR, R-R interval; TE, 3 ms; field of view, 4 cm \times 4 cm; matrix size, 256 \times 256; tagging resolution, 0.5 mm. 15 frames were acquired per cardiac cycle.

Data analysis: Images were analyzed with finite element method. Epicardial and endocardial borders were traced interactively using B-spline interpolation with 8 control points. Intersecting tag points were tracked semi-automatically with HARP-based approach. Subsequently, strains were calculated by 2D homogenous strain analysis. The two eigenvalues of the strain tensor were calculated to yield maximum stretching and maximum shortening. LV torsion was calculated as the differences in the twist between basal and apical slices, normalized by the distance between the two slices.

Cardiomyocyte shortening and calcium transient: Ventricular myocytes were isolated with enzymatic digestion. The cell length during 0.5 Hz electric stimulation was recorded with a Phillips video camera and a Crescent video-edge detector connected to an Olympus IX-71 inverted microscope. Myocytes were loaded with 1 μ M indo-1 AM, and the intracellular calcium was measured by indo-1 emission fluorescence ratio of 410 nm to 480 nm.

Analysis of SR-Associated Calcium Cycling Proteins: Ventricular tissue was homogenized and total protein content was determined by Pierce BCA assay. 20 μ g protein was resolved using standard SDS-PAGE techniques. Protein levels were determined using antibodies against SERCA2a, phospholamban, ryanodine receptor (RyR), and calsequestrin, and detected using the Pierce Supersignal West Femto detection kit. GAPDH was used as loading control.

Results

Global function was similar between $adb^{n-/-}$ mice and the controls. However, $adb^{n-/-}$ mice exhibited significantly enhanced regional deformation from MRI tagging studies. The magnitude of maximum shortening (principal strain) was increased throughout the ventricle in the $adb^{n-/-}$ mice (Fig. 1, left). In accordance with the increased circumferential shortening, the $adb^{n-/-}$ mice also displayed altered LV torsion (Figure 1, right). Peak torsion was $4.3 \pm 0.6^\circ/\text{mm}$ in $adb^{n-/-}$ mice and $3.1 \pm 0.3^\circ/\text{mm}$ in controls ($p < 0.01$).

Isolated cardiomyocytes were characterized to elucidate the cellular changes responsible for changes in regional cardiac function. Figure 2A shows representative changes in cell length during electrical stimulation. Myocyte contractility represented by maximal fractional shortening was significantly increased in the $adb^{n-/-}$ mice ($8.0 \pm 1.5\%$ vs. $6.7 \pm 1.0\%$, $P < 0.01$, Figure 2C). Calcium transient, represented by indo-1 emission ratio, was also significantly increased in $adb^{n-/-}$ myocytes (0.38 ± 0.09 vs. 0.32 ± 0.07 , $p < 0.01$, Figure 2B and 2D). The half relaxation time during calcium uptake was also increased (0.169 ± 0.029 vs. 0.0143 ± 0.027 , $p < 0.01$, Figure 2E).

Western blots observed no significant changes in all the SR-associated calcium cycling protein expressions, suggesting that the altered calcium transient in $adb^{n-/-}$ mice was not caused by SR-associated calcium cycling protein expression. Therefore, it is possible that the DGC associated nNOS regulates calcium homeostasis via the regulation of calcium influx through the sarcolemmal calcium channels.

Conclusion

The $adb^{n-/-}$ mice exhibited an increase in regional ventricular function in vivo. The disruption of DGC signaling via the displacement of nNOS in $adb^{n-/-}$ mice also led to increased cardiomyocyte contractility and calcium release in vitro. Therefore, MRI tagging is sensitive to alterations in myocyte contractility that occur at cellular and molecular levels.

References:

1. Grady R.M. et al, Nature Cell Biology, 1: 215-220, 1999.
2. Yu. X., et al, Pro. Intl. Soc. Mag. Reson. Med. 10 (2002).

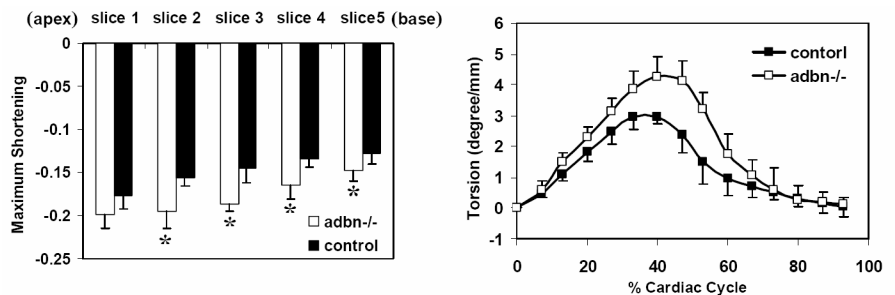


Figure 1. Left: Maximum LV shortening. Right: Time course of LV torsion (* $p < 0.05$).

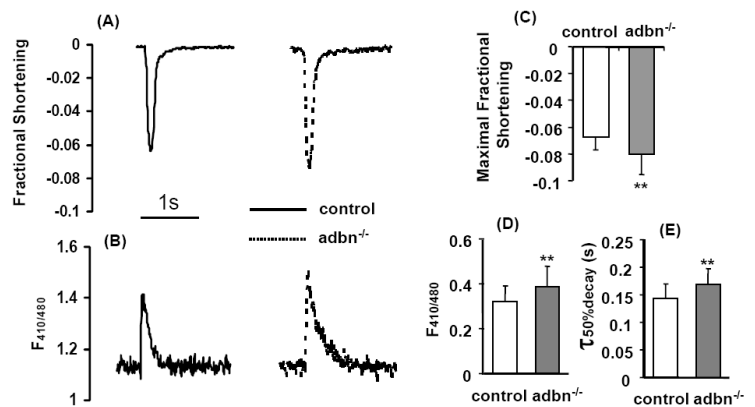


Figure 2. Cardiomyocyte shortening and calcium transient. (A) Representative myocyte fractional shortening; (B) Representative Indo-1 emission fluorescence ratio; (C) Maximum myocyte fractional shortening; (D) Amplitude of indo-1 emission fluorescence ratio; (E) Half relaxation time of calcium transient calculated from indo-1 emission fluorescence ratio curve. (** $p < 0.01$)